Understanding the Features in the Ultrafast Transient Absorption Spectra of CdSe Quantum Dots

Cheng Zhang[†1], Thanh Nhut Do[†1], Xuanwei Ong[2], Yinthai Chan[2,3] and Howe-Siang Tan*[1]

[1] Division of Chemistry and Biological Chemistry, School of Physical and Mathematical Sciences, Nanyang Technological University, 21 Nanyang Link, Singapore 637371

[2] Department of Chemistry, National University of Singapore, 3 Science Drive 3, Singapore 117543

[3] Institute of Materials Research & Engineering, A*STAR, 2 Fusionopolis Way, Innovis, Singapore 138634

* Email address: howesiang@ntu.edu.sg

[†] These authors contributed equally to this work

Key Words: CdSe Quantum Dots, Nonlinear Optical Spectroscopy, Biexcitonic Binding Energy, Femtosecond Spectroscopy

Abstract

We describe a model to explain the features of the ultrafast transient absorption (TA) spectra of CdSe core type quantum dots (QDs). The measured TA spectrum consists of contributions by the ground state bleach (GSB), stimulated emission (SE) and excited state absorption (ESA) processes associated with the three lowest energy transition of the QDs. We model the shapes of the GSB, SE and ESA spectral components after fits to the linear absorption. The spectral positions of the ESA components take into account the biexcitonic binding energy. In order to obtain the correct weightage of the GSB, SE and ESA components to the TA spectrum, we enumerate the set of coherence transfer pathways associated with these processes. From our fits of the experimental TA spectra of 65 Å diameter QDs, biexcitonic binding energies for the three lowest energy transitions are obtained.

1. Introduction

Semiconductor nanocrystals (NCs) have been an important research focus in recent decades due to the great flexibility in their optical and electronic properties. They have been shown to have promising applications in optical detectors [1], solar energy conversion [2] [3], biological sensing [4] and lasers [5]. Among the various types and shapes of NCs are, nearly spherical nanoparticles (quantum dots, QDs) [6], elongated nano-sized crystals (quantum wires or quantum rods) [7] and nanostructures with other shapes such as quantum wells [8]. Semiconductor QDs which are in strongly spatial confinement lead to the discrete distribution of energy levels and result in the rise of interests from researchers both experimentally and theoretically.

Previous works on QDs have provided the static information such as size, shape and surface to reveal structural and optical properties including linear and nonlinear absorption. Recent studies are more focused on the charge carrier dynamics, exciton relaxation or combination pathways and multi-exciton generation and interaction effects by means of varying nonlinear optical techniques [9]. Using time-resolved photoluminescence spectroscopy, single and multi-exciton emission energies and decay dynamics of CdS/ZnSe core/shell type QDs is analyzed to control property of type II QDs with regards to the thickness of the shell [10]. Multi-channel hot exciton relaxation dynamics was reported on colloidal CdSe quantum dots by adopting femtosecond state-resolved pump-probe experiments to study the cooling dynamics and distinguish Auger recombination rate [11]. More recently, multi-dimensional electronic spectroscopy was

applied to study the size and state dynamics [13] and excitonic quantum coherence has been studied [14], [15].

The energy structure in QDs has been described in different level of theories. Ekimov *et al.* reported the model of solving the Hamiltonian of CdSe QDs system with concern given to the degeneracy of valence band and Coulomb interactions between the electrons and the holes [16]. With the model, the three lowest energy states of the holes were determined as $1S_{3/2}$, $1P_{3/2}$ and $2S_{3/2}$, which were well-resolved in the linear absorption spectra of CdSe QDs of various sizes. The study was later shown to be in good agreement with the experimental photoluminescence measurements by Norris *et al.* [17]. In addition, a dark-bright exciton model was put forward to study the temperature dependence of the single-exciton radiative lifetimes [18]-[20], in which the band-edge exciton splitting was described as a result of the strong electron-hole exchange interactions, the asymmetry of the quantum dots and the anisotropies associated with the crystal field.

Ultrafast optical spectroscopy was also performed to explore the biexcitonic dynamics of QDs. However the various prominent features of the TA spectra of QDs have not been adequately explained.

The linear spectrum of the CdSe QDs is dominated by the three lowest energy transitions. Shown in Fig. 1 (a) is the linear spectrum of CdSe QDs with approximately 65 Å diameter, with the positions indicated of the bands of $1S_e - 1S_{3/2}$, $1S_e - 2S_{3/2}$ and $1P_e - 1P_{3/2}$ transitions. These transitions have been previously assigned as X_1, X_2 and X_3, respectively and we adopt the notation of the Caram *et al.* to denote the electronic states

of the CdSe QDs [13], as summarized in the Fig. 1 (b). Overlaid in Fig. 1 (a) is a TA spectrum of the same QDs at 100 ps delay. The negative features of A and B replicates the features of the X_1 and X_2 transition in the linear spectrum. However, at about 2.1 eV, the spectra changed sign and assumes a positive feature C, before going negative again at about 2.22 eV.

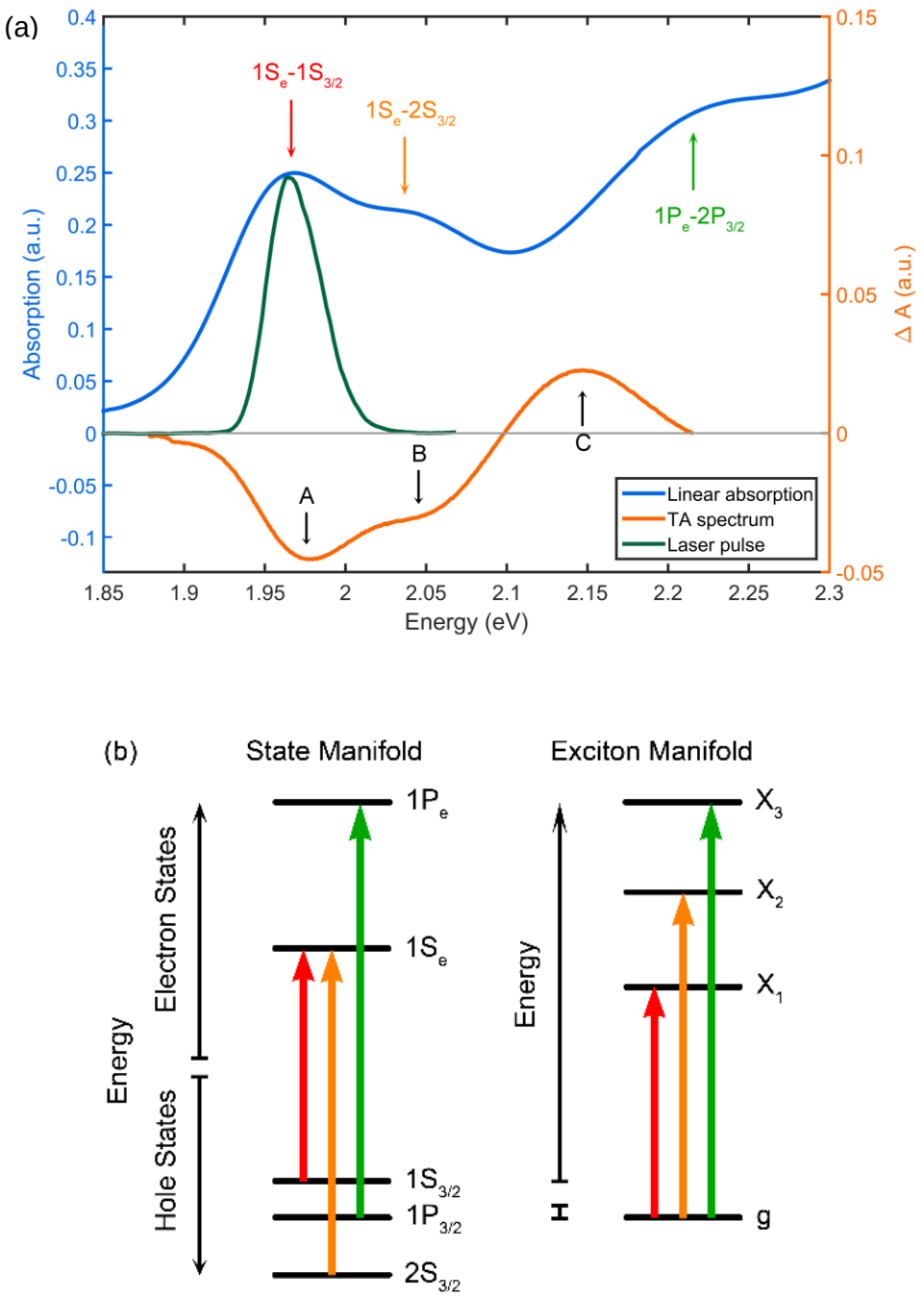

Fig 1. (a) Linear spectrum of CdSe QDs (blue line) overlaid with excitation laser pulse (green line) and TA spectrum at T = 100 ps (orange line); (b) Electronic energy levels of CdSe QDs.

Although the ultrafast TA spectra have previously been studied, the main attention was paid to the band edge, which is associated with the X_1 transition. Klimov used the dynamics of band-edge signal to determine rates of Auger recombination [21]. Sewall *et al.* analyzed the biexcitonic binding energy of the band-edge peak to observe the cooling dynamics of hot excitons [12]. In his study, the transient absorption (TA) spectrum of only the band-edge X_1 transition of the CdSe QDs was discussed.

To the best of our knowledge, we have not came across any articles that attempt to explain the features beyond the band-edge peak (X_1 transition). In this paper, we describe a model to explain the positive and negative features in the TA spectra. The paper is arranged as follows: In section 2, we present the experimental details of the pump-probe measurement to obtain the TA spectra of the CdSe QDs. In section 3, we explain in detail the model that we have used to model the TA spectra. Section 4 presents the fit to the experimental data using the model developed in section 3, and the parameters recovered from the fit. The article ends with a conclusion.

2. Experimental Method

The experimental setup is detailed in former work from our group [22]. Briefly, a commercial Ti:sapphire crystal amplified laser system (Legend Elite, Coherence) with an output pulse centered at 800 nm was used to pump a home-built, double-stage optical parametric amplifier (OPA). After the OPA, a near-infrared output was obtained and frequency-doubled to 630 nm by a BBO crystal. This output is used as our pump pulses and coincide with the band-edge transition of our targeted QDs (Fig. 1). This excitation light is compressed by a commercially acousto-optic programmable pulse shaping unit

(Dazzler, Fastlite) to a pulse duration of 56 fs (1.1 times transform-limited) with 10 nJ energy per pulse. The probe beam then passes through a computer controlled delay stage to generate the delay *T*. The pump beam and the probe beam (parallel in polarization) then overlaps on the sample sealed in a cuvette with 1mm path length. Thereafter, a spectrometer (Acton SP2300) with a CCD detection array (PIXIS 100B) is used to measure the spectrally resolved transient absorption spectrum of the probe beam.

CdSe QDs samples were synthesized according to a procedure previously reported by Chakrabortty *et al*. [23]. With a suitable injection temperature and reaction time, nearly monodisperse QDs with band-edge absorption at ~630 nm were synthesized. The nanoparticles were processed from growth solution via three cycles of precipitation in methanol and re-dispersion in toluene. The processed sample of QDs was then further diluted with toluene to obtain an optical density of 0.2 at the band edge transition.

3. Model

We first model the linear absorption spectra using multi-Gaussian components, based on the theory proposed by Norris [17]. The remaining unresolved absorption continuum, which was considered as the Rayleigh scattering, can be described using a polynomial background term [17]. As indicated in Fig 1, the linear spectrum is dominated by the three lowest electronic transitions of the CdSe QDs, which are $1S_e - 1S_{3/2}$, $1S_e - 2S_{3/2}$ and $1P_e - 1P_{3/2}$ transitions denoted as X_1, X_2 and X_3 respectively. Mathematically, the linear absorption is modelled as

$$A(\omega) = \sum_{i=1}^{3} \alpha_i \exp\left[-\left(\frac{\omega - \omega_i}{\gamma_i} \right)^2 \right] + p_1 + p_2\omega + p_3\omega^2 , \qquad (1)$$

here α_i are the weighted coefficients which are proportional to the absolute square of the transition dipole moments of the respective transitions, ω_i are the center of the Gaussian peaks, γ_i are the factor controlling the Gaussian widths and p_1, p_2 and p_3 are the polynomial coefficients used to model the background terms.

We next discuss the model to describe the TA spectrum. The TA signal spectrum consists of contributions by the ground state bleach (GSB), stimulated emission (SE) and excited state absorption (ESA) processes associated with the X_1, X_2 and X_3 transitions:

$$\Delta A(\omega) = -GSB(\omega) - SE(\omega) + ESA(\omega) . \qquad (2)$$

where $\Delta A(\omega)$ is the TA spectrum. On the right hand side of the equation, the first two terms carry the negative sign and the last term carries the positive sign.

The spectral components of GSB and SE are usually taken to be the same as the linear absorption of the particular transition of interest [12] [24]. The ESA depends on the transition from one excited state to another higher-order excited state (for molecular systems) or multiexcitonic absorptions (for semiconductor systems). In the case of QDs, the ESA corresponds to the transition from a single excitonic state to a biexcitonic state. Due to Coulombic attraction between the excited electron and hole in the single excitonic state, the energy gap for the consecutive transition will be redshifted. This redshift is referred to as the biexcitonic binding energy [11]. The ESA spectrum can therefore be modeled on the basis of the linear absorption spectra redshifted according to the

biexcitonic binding energies. Based on this understanding, the transient absorption spectrum of CdSe QDs is simulated in Sewall's work [12] as:

$$\Delta A(\omega) \propto -2A(\omega) + A(\omega - \Delta_{XX}) \qquad (3)$$

where the former term is twice the linear absorption $A(\omega)$ implying that each transition in the linear spectrum comprises two processes SE and GSB. In Sewall's work, this model was used to model the TA of the band edge which is due to the X_1 excitation only. However, as we will point out below, Eq. $\Delta A(\omega) \propto -2A(\omega) + A(\omega - \Delta_{XX})$ (3) provides an overly simplistic picture, and cannot describe the TA associated with the X_2 and X_3 transitions.

Based on state-filling model presented by Klimov [21], we treat each hole state as spin-doubly degenerated. Moreover, the distinguishability between spin-up and spin-down electrons are taken into consideration. The detailed denotations for amended electronic system are presented in Fig 2.

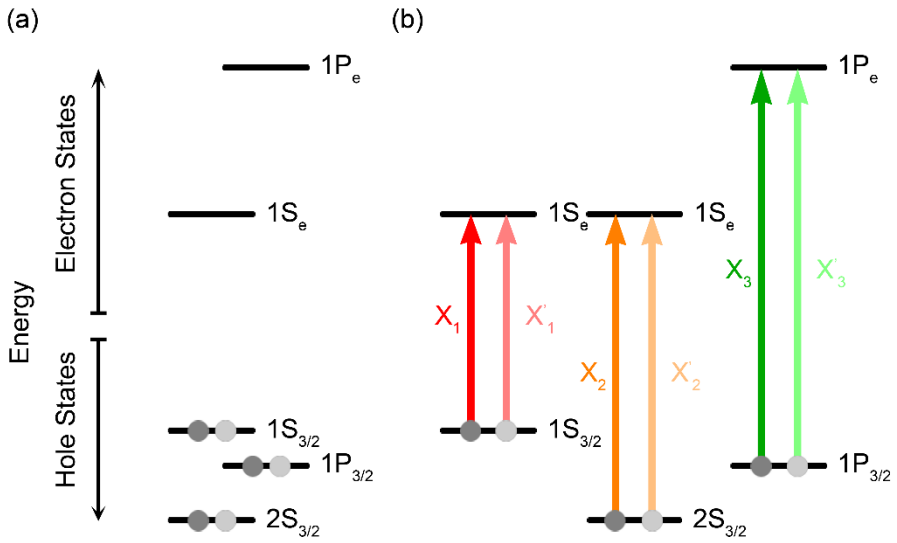

Fig 2. (a) The schematic electronic energy levels of CdSe QDs with each hole state treated as spin-doubly degenerated state; (b) The denotations for electronic transitions with distinguishable spin-up (darker color) and spin-down (lighter color) electrons.

In our experimental condition, the pump pulse is comparatively narrow in the spectral domain (See Fig 1) and we predominantly excite the band edge peak which falls in the X_1 transition, while the probe pulse using a white light continuum is able to probe a much bigger spectral band. Furthermore, it may be assumed that even if the pump has initially excited some parts of the X_2 or X_3 spectral band, after a delay, on the order of 10 ps [25], the population would have decayed to the lowest $1S_e - 1S_{3/2}$ electron-hole state X_1 due to carrier relaxation.

The GSB, SE and ESA processes can be enumerated using Double-sided Feynman Diagrams (DSFDs). The DSFDs are shorthand notations that represent terms from a time dependent perturbative treatment of nonlinear optical response functions.

These terms can be calculated and summed up to give the TA spectrum [26]. Below, we will systematically enumerate the DSFDs for the processes associated with the X_1, X_2 and X_3 transitions. This will then be used to explain the features in the TA spectrum of the QDs.

The TA or pump-probe spectroscopy belongs to the family of third order nonlinear optical spectroscopies. In the language of time dependent perturbation theory that is used to describe such nonlinear optical spectroscopies, the 'pump' pulse interacts twice with the sample, and after a delay of *T*, the 'probe' pulse interacts once. This sets up a third order polarization which then manifest as the signal that emanates in the same direction as the probe pulse. This signal is then heterodyned detected by the 'probe' pulse and frequency resolved detected as the transient absorption spectrum using a spectrometer.

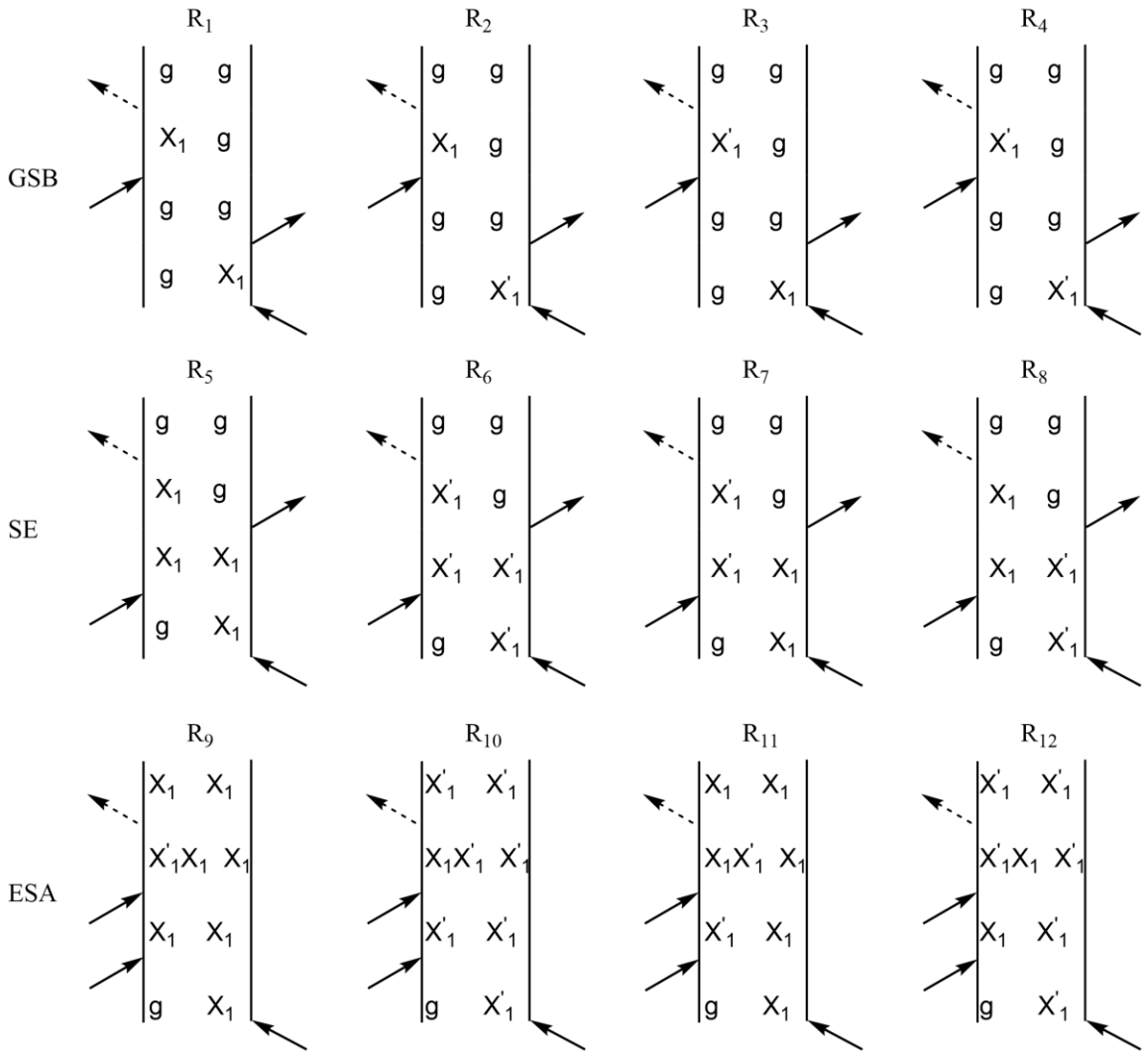

Fig 3. X_1 emission group: DSFDs of all possible rephasing coherence transfer pathways for the GSB, SE and ESA processes associated with the X_1 transition.

In the DFSDs (Fig 3Fig 5), time flows from the bottom to the top, and the density matrix elements are tracked in the center column. The first two interactions are from the pump pulse and the third interaction is from the probe pulse. These interactions are represented by solid line arrows. The last arrow (dashed line) denotes the signal field. Listed in Fig 3Fig 5 are DSFDs for the ‘rephasing’ processes, where the evolution between the first and second interactions involves the off diagonal density matrix element

$|g\rangle\langle X_i|$. There is another set of the same number of DSFDs that belongs to the 'non-rephasing' processes where the evolution between the first and second interactions involves the off diagonal density matrix element $|X_i\rangle\langle g|$, which are not depicted in Fig 3 to Fig 5.

We first consider the DFSDs of the GSB, SE and ESA processes for the X_1 transition in Fig 3. In the first row of Fig 3, we depict the processes that lead to a GSB signal. The second row depicts the processes that lead to a SE signal and the third row enumerates the processes that lead to a ESA signal. Following the sign rules of the DSFDs for the third order signals, GSB and SE processes are proportional to $-\left|\mu_{g\to X_1}\right|^4$ carrying the negative sign while ESA processes are proportional to $\left|\mu_{g\to X_1}\right|^2\left|\mu_{X_1\to X_1X_1'}\right|^2$ which carries a positive sign. $\mu_{g\to X_1}$ is the transition dipole moment for the transition to a single exciton state ($g\to X_1$) while $\mu_{X_1\to X_1X_1'}$ is the transition dipole moments for the transition to a biexcitonic state ($X_1\to X_1X_1'$). Assuming simplistically that the values of $\mu_{g\to X_1}$ and $\mu_{X_1\to X_1X_1'}$ to be the same, all the DSFDs will have similar amplitudes. Taking these into consideration, one can conclude that there is a ratio of 2 to 1 between the negative (GSB and SE) and positive signals (ESA).

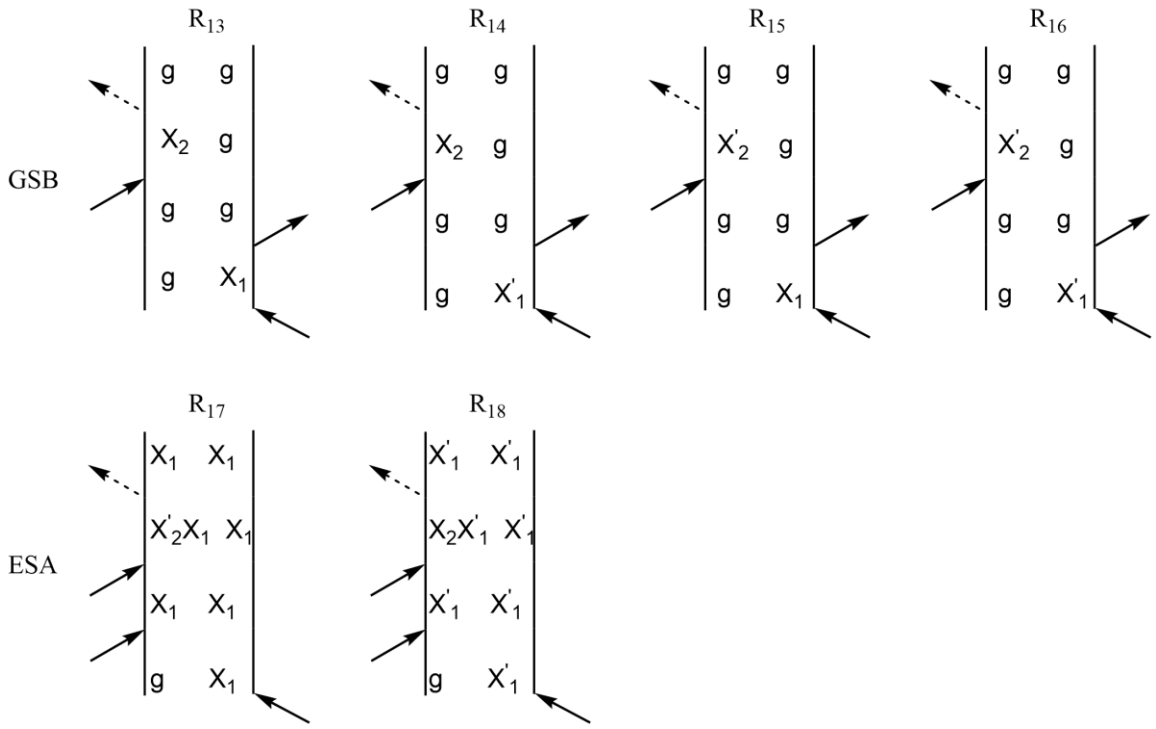

Fig 4. X_2 emission group: DSFDs of all possible rephasing coherence transfer pathways for GSB and ESA processes associated with the X_2 transition.

We now discuss the TA signal contributed by the X_2 transitions (shown in Fig 4). In the first row, the GSB signals are similar to the X_1 case as presented in Fig 3. However, there is no SE signals. This is due to the fact that there is no excited population in the X_2 state. For the ESA signal, we need to take into consideration the Pauli exclusion principle. The X_1 ($1S_e - 1S_{3/2}$) and X_2 ($1S_e - 2S_{3/2}$) transitions share the same electron state. Therefore, after the 'pump' excitation, if the electron state $1S_e$ is populated with a spin-up electron of the $1S_e - 1S_{3/2}$ transition (denoted as X_1), the 'probe' can only excite the spin-down electron of the $1S_e - 2S_{3/2}$ transition (denoted as X_2') and vice-versa. Essentially we can only reach the biexcitonic states $\left|X_2X_1^{'}\right\rangle$ or $\left|X_2^{'}X_1\right\rangle$. This restriction leads to fewer number of DSFDs for the ESA signals as shown in Fig 4. One can then

conclude that the ratio between negative (GSB) and positive signals (ESA) is still the same as the X_1 case, namely 2 to 1.

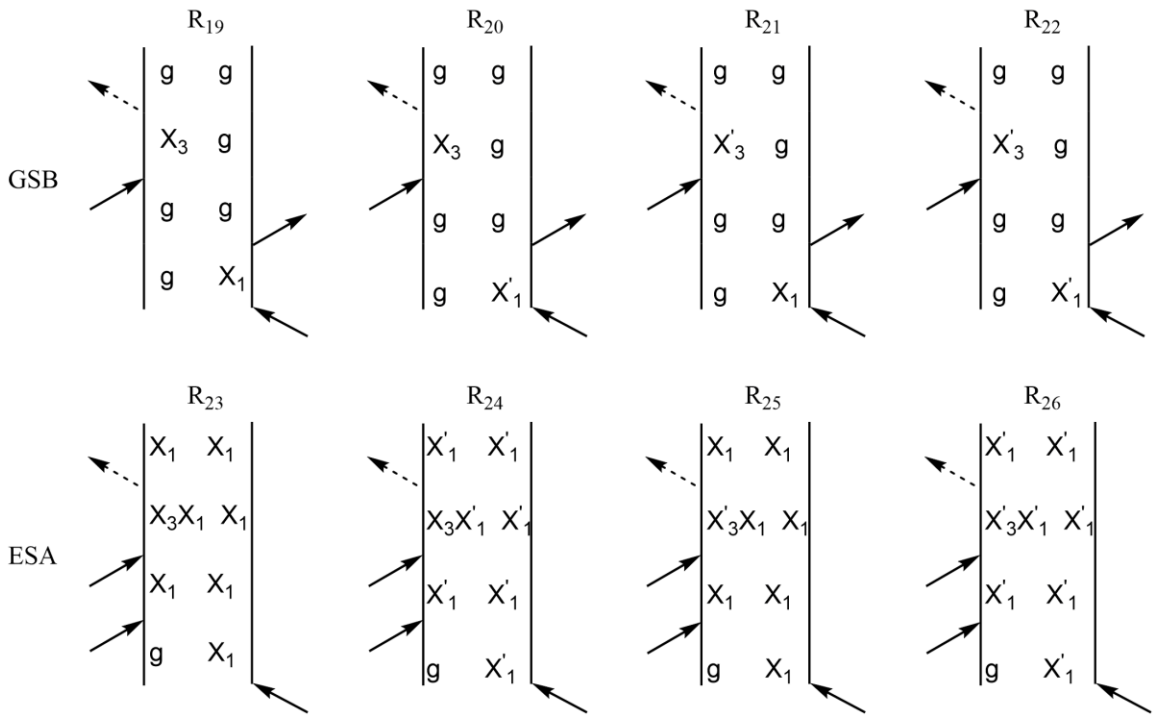

Fig 5. X_3 emission group: DSFDs of all possible rephasing coherence transfer pathways for GSB and ESA processes associated with the X_3 transition.

We now discuss the TA signal contributed by the X_3 transitions (shown in Fig 5). Analogous to transitions associated with X_2, there is no SE signal. However, in this case, the X_1 ($1S_e - 1S_{3/2}$) and X_3 ($1P_e - 1P_{3/2}$) do not share the same electron state. Subsequently, the 'probe' pulse can excite a total of four combinations between spin-up and spin-down electrons of X_1 and X_3 transitions described by 4 DSFDs in the second row of Fig 5. Taking this into consideration, there is two more ESA DSFDs compared to the X_2 case. This results in the ratio of negative (GSB) to positive (ESA) signals to be 1 to 1.

We now describe the numerical modelling of the TA spectrum as described in Eq. 2. For the GSB signals for X_1, X_2, and X_3, we use the Gaussian functions obtained from the fit of linear spectrum as described in Eq. 1:

$$GSB(\omega) \propto \sum_{i=1}^{3} \alpha_i \exp\left[-\left(\frac{\omega-\omega_i}{\gamma_i}\right)^2\right]. \quad (4)$$

The SE pathways which only appears in X_1 emission group (Fig 3) is expressed as:

$$SE(\omega) \propto \alpha_1 \exp\left[-\left(\frac{\omega-\omega_1}{\gamma_1}\right)^2\right] \quad (5)$$

The ESA signal can be interpreted as arising from the single excitonic to biexcitonic transition (X→XX), which is redshifted from single excitonic transitions (g→X) by a biexcitonic binding energy, $\Delta_i = E_{X_1} + E_{X_i} - E_{X_1X_i}$, where E_{X_1} is the energy of the X_1 state, E_{X_i} is the energy of the X_i state and $E_{X_1X_i}$ is the energy of the biexcitonic X_1X_i state. This biexcitonic binding energy arises from Coulomb interactions caused by the excited electron and hole pair. With the ratio of GSB and SE signal to ESA derived earlier, the contribution of the ESA spectrum can be expressed as

$$\begin{aligned} ESA(\omega) \propto \alpha_1 \exp\left[-\left(\frac{\omega-\omega_1+\Delta_1}{\gamma_1}\right)^2\right] + \frac{1}{2}\alpha_2 \exp\left[-\left(\frac{\omega-\omega_2+\Delta_2}{\gamma_2}\right)^2\right] \\ +\alpha_3 \exp\left[-\left(\frac{\omega-\omega_3+\Delta_3}{\gamma_3}\right)^2\right] \end{aligned}. \quad (6)$$

The first term in Eq. 6 represents the X_1 emission group and it is the same as the term in SE and GSB signals because there are equal number of accessible ESA processes compared with GSB and SE processes. However, in the X_2 emission group (Fig 4), the ESA processes are only half of the GSB pathways due to Pauli exclusion principle. So a factor of ½ appears in the second term in ESA contribution of Eq. 6. Similarly, the last term, which represents the X_3 emission group, shares the same weight as the respective GSB processes.

Taking into consideration all the terms in Eq. 4, 5 and 6, the transient absorption spectrum of CdSe QDs is modelled using the formula below

$$\begin{aligned}\Delta A(\omega) \propto & -\sum_{i=1}^{3}\alpha_i \exp\left[-\left(\frac{\omega-\omega_i}{\gamma_i}\right)^2\right]-\alpha_1 \exp\left[-\left(\frac{\omega-\omega_1}{\gamma_1}\right)^2\right] \\ & +\alpha_1 \exp\left[-\left(\frac{\omega-\omega_1+\Delta_1}{\gamma_1}\right)^2\right]+\frac{1}{2}\alpha_2 \exp\left[-\left(\frac{\omega-\omega_2+\Delta_2}{\gamma_2}\right)^2\right]. \\ & +\alpha_3 \exp\left[-\left(\frac{\omega-\omega_3+\Delta_3}{\gamma_3}\right)^2\right]\end{aligned} \qquad (7)$$

where the first negative summation represents the GSB spectrum and the second negative term stands for the SE signals, while the next three positive terms are ESA signals.

Qualitatively, we can now explain the trends of the TA spectrum lineshape. As depicted in Fig 6, the negative peaks represent GSB and SE signals and the positive peaks are ESA signals. In Fig 6 (a), with the 2 to 1 ratio of negative and positive signals, the TA lineshapes of features A and B are demonstrated. With the negative peak representing GSB and SE centered at the linear absorption maximum and the positive ESA peak

redshifted by the biexcitonic binding energy, the TA lineshape is an asymmetric negative peak approximately replicating the linear absorption peak. On another hand, if the amplitudes of negative and positive signals are equal as in the case for the X_3 emission group (Fig 5), the resultant TA lineshape has a 'dispersive' profile as depicted in Fig 6 (b). The feature C in TA spectra shown in Fig 1 (a) is the positive half of this dispersive line. The other negative half is not resolved due to the limitation of probe pulse spectral range.

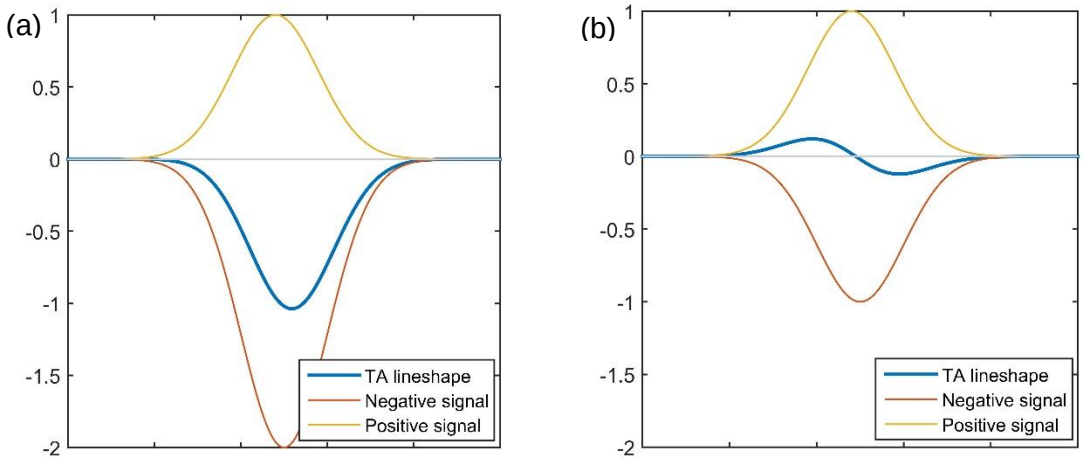

Fig 6. (a) TA lineshape for features A and B of Fig 1 (a) with the ratio between negative and positive signal being 2 to 1. (b) TA lineshape for feature C with the ratio between negative and positive signal being 1 to 1.

4. Results and Discussion

We apply our proposed model to the experimental collected linear absorption spectrum. The results are plotted in Fig 7 with $R^2 > 0.99995$ and the root-mean-square-error (RMSE) around 3.97×10^{-4}. We can see that the simulated spectrum is a reasonable

fit to the experimental data. The linewidth of each transition increases with the growth of energy from X_1 to X_3. This broadening is consistent with previous works done by Norris [17], Bawendi [27], and Hoheisel [28].

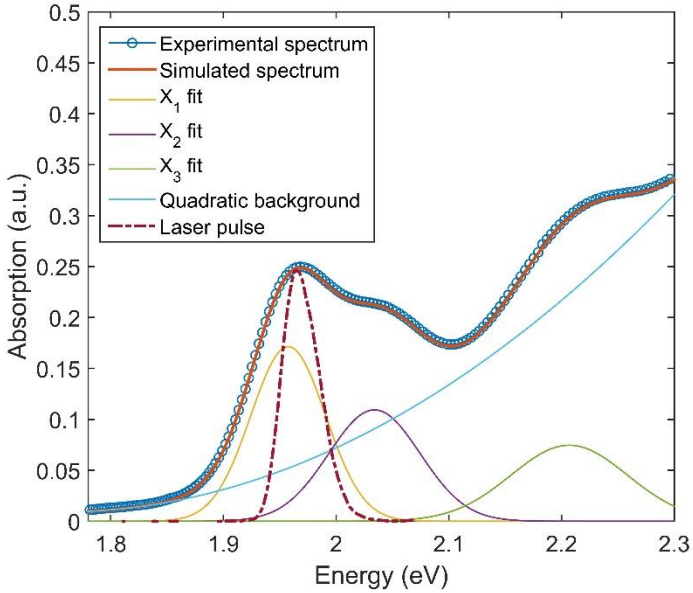

Fig 7. Linear spectrum of CdSe QDs overlaid with the excitation laser pulse and the fitted functions presented in Eq. 7.

From the fitting results, we can determine that the transition energies of the X_1, X_2 and X_3 are 1.96, 2.03, and 2.21 eV, respectively.

Although there is an overlap between the pump excitation spectrum and the X_2 state (Fig 7.), the resultant excited population in the X_2 transition is much smaller than the one in the X_1 transition (See Supplementary Information I). Furthermore, through carrier relaxation, all the population would have decayed to the $1S_e - 1S_{3/2}$ electron-hole

state and spectral diffusion has resulted in the redistribution over the whole of the X_1 band (See Supplementary Information II) by T = 10 ps [25], therefore we are only including TA spectra for T > 10 ps in our studies here.

Referring to the analysis in the Model section, the TA spectrum of CdSe QDs with T = 100 ps is fit with Eq. 7. The results of the fit are depicted in Fig 8 with R^2 = 0.9238 and RMSE = 0.0060. We can see the obvious deviation between the experimental and the simulation results. In addition, the fitting results return the values of biexcitonic binding energy of Δ_1 = 7.45 ± 4.21 meV, Δ_2 = 78.43 ± 14.89 meV, and Δ_3 = 41.84 ± 4.55 meV, which are not physically reasonable because previous studies in Ref [12], [21] and [29] indicated that biexcitonic binding energy cannot be as large as 70 meV.

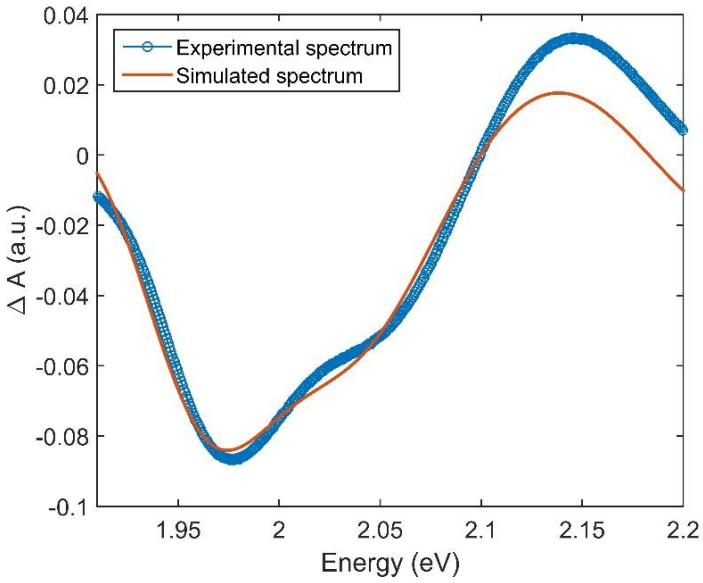

Fig 8. Comparing the simulated transient absorption spectrum with the experimental transient absorption spectrum.

Hitherto, we have assumed that the transition dipole moments $\mu_{X_1 \to X_1 X_1'}$ for the transition to a biexcitonic state (X→XX) to be the same as the transition to a single exciton state (g→X) $\mu_{g \to X_1}$. We relax this condition and allow the ESA processes to undergo the transitions with different transition dipole moments. In this case, we modify the model for transient absorption spectrum to become:

$$\begin{aligned}\Delta A(\omega) \propto & -\sum_{i=1}^{3} \alpha_i \exp\left[-\left(\frac{\omega-\omega_i}{\gamma_i}\right)^2\right] - \alpha_1 \exp\left[-\left(\frac{\omega-\omega_1}{\gamma_1}\right)^2\right] \\ & + \alpha_1 m_1 \exp\left[-\left(\frac{\omega-\omega_1-\Delta_1}{\gamma_1}\right)^2\right] + \frac{1}{2}\alpha_2 m_2 \exp\left[-\left(\frac{\omega-\omega_2-\Delta_2}{\gamma_2}\right)^2\right] \\ & + \alpha_3 m_3 \exp\left[-\left(\frac{\omega-\omega_3-\Delta_3}{\gamma_3}\right)^2\right]\end{aligned} \qquad (8)$$

where m_i is the ratio between the absolute squares of the transition dipole moments $m_i = \left|\mu_{X_1 \to X_1 X_i'}\right|^2 \Big/ \left|\mu_{g \to X_1}\right|^2$. These parameters account for the change of transition dipole moments caused by the perturbation of excitation. Using the modified model, the transient absorption spectrum at T = 100 ps is fit with non-linear-least-square method.

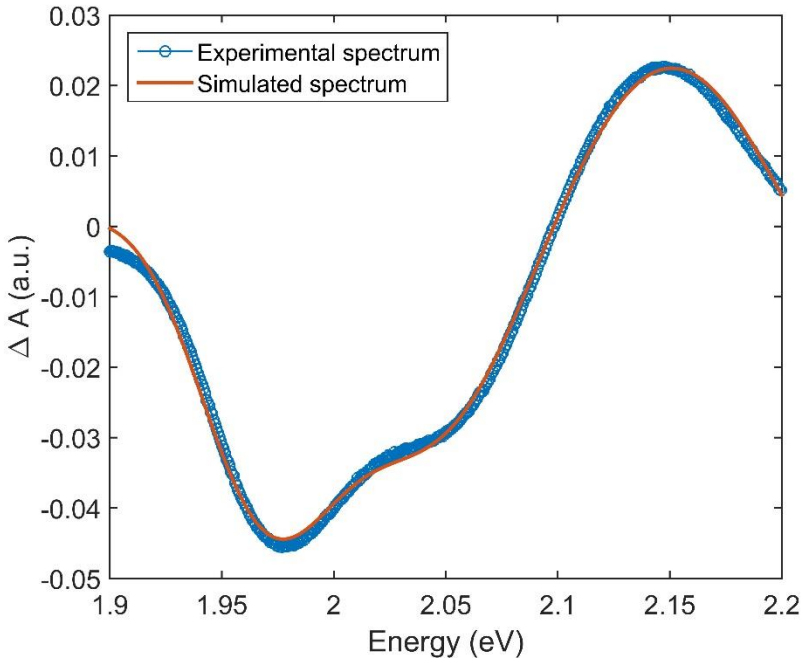

Fig 9. Comparing the experimental with the simulated transient absorption spectrum using the modified model on CdSe QDs.

The resultant fitting is much better than the previous fit, with R^2 = 0.9962 and RMSE = 0.0013. The resultant biexcitonic binding energy values are Δ_1 = 3.179 ± 0.512 meV, Δ_2 = 9.18 ± 2.27 meV, and Δ_3 = 28.09 ± 2.27 meV. This results is consistent with previous studies [12], [21], [29]. The fit for the m_i values are all greater than 1 (See Table 1) implying that the transition dipole moment is greater for the transition to a biexcitonic state (X→XX) than the corresponding transition to a single exciton state (g→X). This can be rationalize by the increasing of overlap between electron and hole wavefunctions in the biexcitonic states [30], [31]. Our values are consistent with the study conducted by Takagahara which concludes that the oscillator strength (which is proportional to the absolute square of transition dipole moment) ratio between biexcitonic and

monoexcitonic transition $m_i = \left|\mu_{X_1 \to X_1 X_i'}\right|^2 \Big/ \left|\mu_{g \to X_1}\right|^2$ has a typical value around 1 to 2.5 [30].

We also conduct the global fitting for all data having *T* ranged between 10 – 900 ps. All TA spectra within this *T* range are normalized to eliminate the population decay dynamics. The fitting is conducted over the entire data set and the summarized results are presented below:

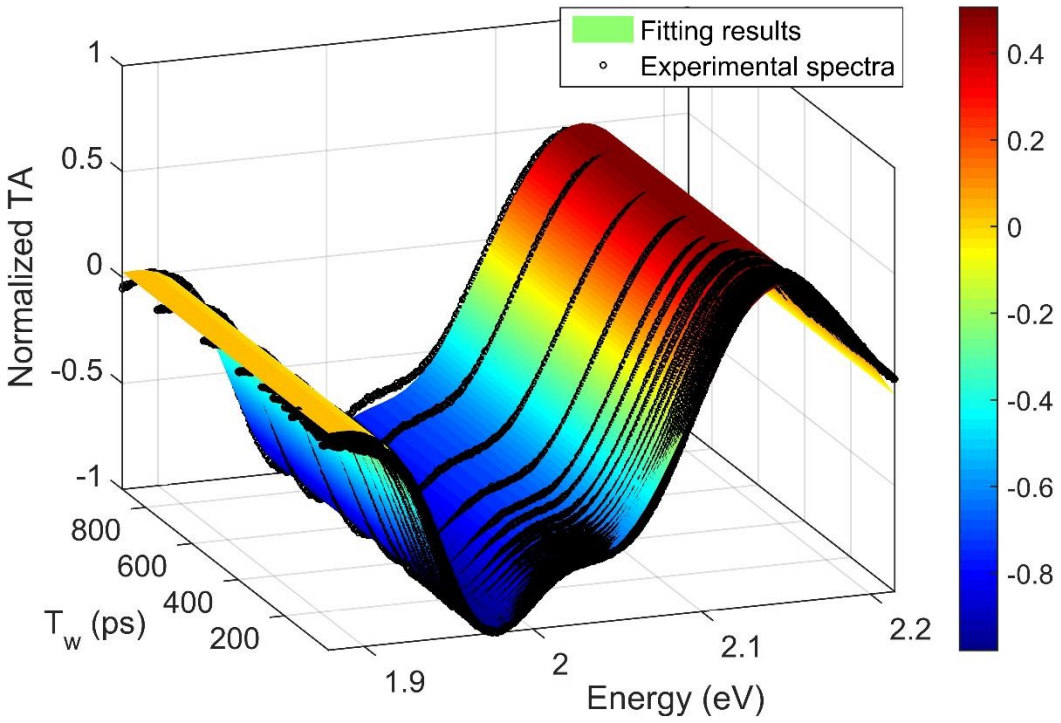

Fig 10. Normalized global fitting results of TA spectra with *T* ranging from 10 ps to 900ps.

Table 1. Summarized fitting results of TA spectra

Model	Fitting result	R^2	RMSE
Original model ($m_i = \left\|\mu_{X_1 \to X_1 X_i'}\right\|^2 / \left\|\mu_{g \to X_1}\right\|^2 = 1$)	Δ_1 = 7.45 ± 4.21 meV Δ_2 = 78.43 ± 14.89 meV Δ_3 = 41.84 ± 4.55 meV	0.9238	0.0060
Modified model ($m_i = \left\|\mu_{X_1 \to X_1 X_i'}\right\|^2 / \left\|\mu_{g \to X_1}\right\|^2 \neq 1$)	Δ_1 = 3.179 ± 0.512 meV Δ_2 = 9.18 ± 2.27 meV Δ_3 = 28.09 ± 2.27 meV m_1 = 1.689 ± 0.042 m_2 = 1.267 ± 0.088 m_3 = 1.175 ± 0.036	0.9962	0.0013
Modified model (Global fitting of TA spectra, T = 10 – 900 ps) ($m_i = \left\|\mu_{X_1 \to X_1 X_i'}\right\|^2 / \left\|\mu_{g \to X_1}\right\|^2 \neq 1$)	Δ_1 = 3.422 ± 0.084 meV Δ_2 = 9.716 ± 0.358 meV Δ_3 = 28.25 ± 0.35 meV m_1 = 1.693 ± 0.007 m_2 = 1.290 ± 0.013 m_3 = 1.180 ± 0.006	0.9956	0.0318

The values obtained from the range of delays from 10 ps to 900 ps are very similar. The trends of the biexcitonic binding energies and transition dipole moments values obtained from our fits are in broad agreement with the values reported in the literature. However as the optimization of the values are interdependent in our fit, the set

of values recovered for biexcitonic binding energies and transition dipole moments ratio values may not be unique. Additional studies, such as the theoretical calculations of the biexcitonic binding energies and transition dipole moments values will help us narrow the range of values for the fit. Further experiments using technique such as 2DES will be able to help us clarify the contribution of homogeneity, inhomogeneity and spectral diffusion to the spectral features [32].

5. Conclusion

Using a simple model, we were able to explain the negative and positive features in the TA spectrum (1.9 eV to 2.2 eV) of CdSe quantum dots with 65 Å diameter. We provide a model to fit the TA spectra. This is done by a careful enumeration of all GSB, SE and ESA processes associated with the three lowest energy transitions $1S_e - 1S_{3/2}$, $1S_e - 2S_{3/2}$ and $1P_e - 1P_{3/2}$. We then introduced global fitting in our model to fit our experimental TA spectra. We obtain the biexcitonic binding energies, corresponding to the $1S_e - 1S_{3/2}$, $1S_e - 2S_{3/2}$ and $1P_e - 1P_{3/2}$ states as 3.4, 9.7 and 28 meV, respectively. These results are in general agreement with literature values.

Due to the strong spatial confinement in semiconductor NCs, especially in QDs, the strength of electron-hole Coulomb interactions are significantly enhanced compared with their counterparts in bulk semiconductor [21]. So it is of great importance to determine multi-exciton binding energies since it is a direct indicator on the strength of Coulomb interactions contributions. It is hoped that this model enables us to gain better information of the contributions from above mentioned processes.

Acknowledgements

This work is supported by a grant from the Singapore Ministry of Education Tier 2 Academic Research Fund (MOE2015-T2-1-039).

References

[1] M. Kroner, K. M. Weiss, B. Biedermann, S. Seidl, S. Manus, A. W. Holleitner, A. Badolato, P. M. Petroff, B. D. Gerardot, R. J. Warburto, and K. Karrai, Optical Detection of Single-Electron Spin Resonance in a Quantum Dot, *Phys. Rev. Lett.*, **100**, 156803 (2008).

[2] P. V. Kamat, Meeting the Clean Energy Demand: Nanostructure Architectures for Solar Energy Conversion, *J. Phys. Chem. C*, **111**, 2834 (2007).

[3] P. V. Kamat, Quantum Dot Solar Cells. The Next Big Thing in Photovoltaics, *Phys. Chem. Lett.*, **4**, 908 (2013).

[4] S. J. Peartona, F. Renb, Y. L. Wangb, B. H. Chub, K. H. Chenb, C. Y. Changb, W. Lima, J. Linc, and D. P. Nortona, Recent Advances in Wide Bandgap Semiconductor Biological and Gas Sensors, *Prog. Mater. Sci.*, **55**, 1 (2010).

[5] B. Ellis, M. A. Mayer, G. Shambat, T. Sarmiento, J. Harris, E. E. Haller, and J. Vučković, Ultralow-threshold Electrically Pumped Quantum-dot Photonic-crystal Nanocavity Laser, *Nat. Photonics*, **5**, 297 (2011).

[6] L. Qu, and X. Peng, Control of Photoluminescence Properties of CdSe Nanocrystals in Growth, *J. Am. Chem. Soc.*, **124**, 2049 (2002).

[7] X. Peng, L. Manna, W. Yang, Wickham J, E. Scher, A. Kadavanich, and A. P. Alivisatos, Shape Control of CdSe Nanocrystals, *Nature*, **404**, 59 (2000).

[8] M.E. Mora-Ramosa, C.A. Duqueb, E. Kasapogluc, H. Saric, and I. Sökmen, Linear and Nonlinear Optical Properties in a Semiconductor Quantum Well under Intense Laser Radiation: Effects of Applied Electromagnetic Fields, *J. Lumin.*, **132**, 901 (2012).

[9] D. A. Wheeler, J. Z. Zhang, Exciton Dynamics in Semiconductor Nanocrystals, *Adv. Mater.*, **25**, 2878 (2013).

[10] S. A. Ivanov, and M. Achermann, Spectral and Dynamic Properties of Excitons and Biexcitons in Type-II Semiconductor Nanocrystals, *ACS Nano*, **4**, 5994 (2010).

[11] P. Kambhampati, Hot Exciton Relaxation Dynamics in Semiconductor Quantum Dots: Radiationless Transitions on the Nanoscale, *J. Phys. Chem. C.*, **115**, 22089 (2011).

[12] S. L. Sewall, R. R. Cooney, E. A. Dias, P. Tyagi, and P. Kambhampati, State-Resolved Observation in Real Time of the Structural Dynamics of Multiexcitons in Semiconductor Nanocrystals, *Phys. Rev. B.*, **84**, 235304 (2011).

[13] J. R. Caram, H. Zheng, P. D. Dahlberg, B. S. Rolczynski, G. B. Griffin, D. S. Dolzhnikov, D. V. Talapin, and G. S. Engel, Exploring Size and State Dynamics in CdSe Quantum Dots Using Two-Dimensional Electronic Spectroscopy, *J. Chem. Phys.* **140**, 084701 (2014).

[14] J. R. Caram, H. Zheng, P. D. Dahlberg, B. S. Rolczynski, G. B. Griffin, A. F. Fidler, D. S. Dolzhnikov, D. V. Talapin, and G. S. Engel, Persistent Interexcitonic Quantum Coherence in CdSe Quantum Dots, *J. Phys. Chem. Lett.*, **5**, 196 (2014).

[15] S. Dong, D. Trivedi, S. Chakrabortty, T. Kobayashi, Y. Chan, O. V. Prezhdo, and Z.-H. Loh, Observation of an Excitonic Quantum Coherence in CdSe Nanocrystals, *Nano Lett.*, **15**, 6875 (2015).

[16] A. I. Ekimov, F. Hache, M. C. Schanne-Klein, D. Ricard, C. Flytzanis, I. A. Kudryavtsev, T. V. Yazeva, A. V. Rodina, and Al. L. Efros, Absorption and Intensity-Dependent Photoluminescence Measurements on CdSe Quantum Dots: Assignment of the First Electronic Transitions, *J. Opt. Soc. Am. B.*, **10**, 100 (1993).

[17] D. J. Norris, and M. G. Bawendi, Measurement and Assignment of the Size-Dependent Optical Spectrum in CdSe Quantum Dots, *Phys. Rev. B.*, **53**, 16338 (1996).

[18] M. Nirmal, D. J. Norris, M. Kuno, M. G. Bawendi, A. L. Efros, and M. Rosen, Observation of the "Dark Exciton" in CdSe Quantum Dots, *Phys. Rev. Lett.*, **75**, 3728 (1995).

[19] S. A. Crooker, T. Barrick, J. A. Hollingsworth, and V. I. Klimov, Multiple Temperature Regimes of Radiative Decay in CdSe Nanocrystal Quantum Dots: Intrinsic Limits to the Dark-Exciton Lifetime, *Appl. Phys. Lett.*, **82**, 2793 (2003).

[20] O. Labeau, P. Tamarat, and B. Lounis, Temperature Dependence of the Luminescence Lifetime of Single CdSe/ZnS Quantum Dots, *Phys. Rev. Lett.*, **90**, 257404 (2003).

[21] V. I. Klimov, Spectral and Dynamical Properties of Multiexcitons in Semiconductor Nanocrystals, *Annu. Rev. Phys. Chem.*, **58**, 635 (2007).

[22] Z. Zhang, K. L. Wells, E. W. J. Hyland, H-S. Tan, Phase-cycling Schemes for Pump–Probe Beam Geometry Two-Dimensional Electronic Spectroscopy, *Chem. Phys. Lett.*, **550**, 156 (2012).

[23] S. Chakrabortty, G. Xing, Y. Xu, S. W. Ngiam, N. Mishra, T. C. Sum, Y. Chan, Engineering Fluorescence in Au-Tipped, CdSe-Seeded CdS Nanoheterostructures, *Small*, **7**, 2847 (2011).

[24] R. Berera, R. van Grondelle, and J. T. M. Kennis, Ultrafast Transient Absorption Spectroscopy: Principles and Application to Photosynthetic Systems, *Photosynth. Res.*, **101**, 105 (2009).

[25] P. Kambhampati, Hot Exciton Relaxation Dynamics in Semiconductor Quantum Dots: Radiationless Transitions on the Nanoscale, *J. Phys. Chem. C*, **115**, 22089 (2011).

[26] P. Hamm, *Principles of Nonlinear Optical Spectroscopy: A Practical Approach* (University of Zurich, 2005).

[27] M. G. Bawendi, W. L. Wilson, L. Rothberg, P. J. Carroll, T. M. Jedju, M. L. Steigerwald, and L. E. Brus, Electronic Structure and Photoexcited-Carrier Dynamics in Nanometer-Size CdSe Clusters, *Phys. Rev. Lett.*, **65**, 1623 (1990).

[28] W. Hoheisel, V. L. Colvin, C. S. Johnson, and A. P. Alivisatos, Threshold for Quasicontinuum Absorption and Reduced Luminescence Efficiency in CdSe Nanocrystals, *J. Chem. Phys.*, **101**, 8455 (1994).

[29] N. Lenngren, T. Garting, K. Zheng, M. Abdellah, N. Lascoux, F. Ma, A. Yartsev, K. Zidek, and T. Pulleris, Multiexciton Absorption Cross Sections of CdSe

Quantum Dots Determined by Ultrafast Spectroscopy, *J. Phys. Chem. Lett.*, **4**, 3330 (2013).

[30] T. Takagahara, Biexciton States in Semiconductor Quantum Dots and Their Nonlinear Optical Properties, *Phys. Rev. B*, **39**, 10206 (1989).

[31] M. Sahin, and F. Koç, A Model for the Recombination and Radiative Lifetime of Trions and Biexcitons in Spherically Shaped Semiconductor Nanocrystals, *Appl. Phys. Lett.*, **102**, 183103 (2013).

[32] O. Rancova, and D. Abramavicius, Static and Dynamic Disorder in Bacterial Light-Harvesting Complex LH2: A 2DES Simulation Study, *J. Phys. Chem. B*, **118**, 7533 (2014).